Role of Charge Ordering in the Dynamics of Cluster Formation in Associated Liquids

Bernarda Lovrinčević, Martina Požar, Ivo Jukić, Aurélien Perera

On the role charge ordering in the dynamics of cluster formation in associated liquids

Bernarda Lovrinčević[‡*], Martina Požar[‡], Ivo Jukić[†,‡ ¦] and Aurélien Perera[†‡]

June 1, 2023

[‡]University of Split, Faculty of Science, Ruđera Boškovića 33, 21000, Split, Croatia.

[†]Laboratoire de Physique Théorique de la Matière Condensée (UMR CNRS 7600), Sorbonne Université, 4 Place Jussieu, F75252, Paris cedex 05, France.

Abstract

Liquids are archetypes of disordered systems, yet liquids of polar molecules are locally more ordered than non-polar molecules, due to the Coulomb interaction based charge ordering phenomenon. Hydrogen bonded liquids, such as water or alcohols, for example, represent a special type of polar liquids, in that they form labile clustered local structures. For water, in particular, hydrogen bonding and the related local tetrahedrality, play an important role in the various attempts to understand this liquid. However, labile structures imply dynamics, and it is not clear how it affects the understanding of this type of liquids from purely static point of view. Herein, we propose to reconsider hydrogen bonding as a charge ordering process. This concept allows to demonstrate the insufficiency of the analysis of the microscopic structure based solely on static pair correlation functions, and the need for dynamical correlation functions, both in real and reciprocal space. The subsequent analysis allows to recover several aspects of our understanding of hydrogen bonded liquids, but from the charge order perspective. For water, it confirms the jump rotation picture found recently, and it allows to rationalize the contradicting pictures that arise when following the interpretations based on hydrogen bonding. For alcohols, it allows to understand the dynamical origin of the scattering pre-peak, which does not exist for water, despite the fact that both these liquids have very similar hydroxyl group chain clusters. The concept of charge ordering complemented by the analysis of dynamical correlation functions appear as a promising way to understand micro-heterogeneity in complex liquids and mixtures from kinetics point of view.

[*]bernarda@pmfst.hr

[†]Doctoral School of Biophysics, University of Split, Croatia

[‡]corresponding author (aup@lptmc.jussieu.fr)

1 Introduction

Interactions in liquids, when addressed from classical point of view, come mostly in two categories, short ranged dispersion interactions such as the canonical Lennard-Jones interactions, and long ranged Coulomb interactions [1]. These interactions produce very different forms of local order, the former being close to perfect disorder, typically in a Lennard-Jones simple liquid, while the charge order of the latter leads to the peculiar checker board type form of local order [2, 3, 4, 5, 6], typically seen in molten salts [7, 8, 9]. When considering complex molecules, whether these are ionic, polar or non-polar, they are all made of non-charged and charged atomic groups, and charge order still dominates the local molecular order, according to the same two features mentioned above. When considering the sub-group of molecules which can form hydrogen bonds, such as water and alcohols, for example, or other types of bond, these can can also be described in term of charge order, since many classical force fields built solely with the above mentioned two types of interactions, often suffice to describe both the structure and thermo-physical properties of many molecular liquids with acceptable accuracy [10]. Even though hydrogen bonding originates from quantum mechanics, there is an enormous corpus of published material, specifically concerning water, using classical force field simulation [11, 12, 13], which support the idea that the charge order hypothesis equally apply to such complex liquids.

The charge order hypothesis is interesting for several reasons. First of all, it transfers the polar/apolar paradigm [14, 15], which is focused on dipolar properties, to charged/uncharged paradigm, which is about individual atomic sites. This is interesting since it allows to use site-site correlation functions, instead of orientational correlation functions, the latter which involve much more variables. Secondly, and this is the main focus of this paper, it allows to rationalize the duality of fluctuations and micro-segregation found in many Hbonding systems and mixtures, and which concerns the existence of labile Hbonded clusters [16, 17, 18, 19]. While our previous work focused on static structural properties [20, 21, 22], the present work focus is on the dynamical ones, with the idea to separate the cluster kinetics time from the molecular relaxation times, and how this is related to static cluster signatures, such as the scattering pre-peak for instance [23, 24]. Herein, we would like to examine the problem posed by the influence of the local structure of hydrogen bonded labile clusters on the global understanding of these liquids, under two different perspectives, one based of charge order arguments, and the other on the importance of the dynamics of the labile structures.

The fact that the existence of Hbonded clusters and their dynamics influences greatly the thermo-physical properties has been numerously addressed in the past, in specific contexts, and we briefly review some of them. Water has been the most important target to study this problematic, with issues such as a large amount of anomalies scattered all over the phase diagram [25, 26, 27], debates about the existence of a second critical point in the supercooled states [28, 29, 30, 31, 32, 33], or the issue of whether or not water is a "special" liquid

different from a simple LJ liquid [34, 35, 36], particularly in what concerns its role in biological issues [37]. Perhaps the issue closest to ours is that which concerns the existence of two type of water local structure, an idea which dates back to Roentgen [38], and, since the earlier works of Franck [39], has been revived several times [40, 25]. Interestingly, these problems about water structure oscillate between investigating the instantaneous microstructure, which is part of the microstates, and averaged macrostate approach, such as concerning the study of pair correlation functions [41, 42, 43, 44]. The first type of approach has been put forward recently through machine learning approaches [45].

These studies differ from ours in perspective, in spite of many overlaps concerning particular details. Indeed, our interest is about the duality of fluctuations and micro-heterogeneity [46, 22, 47]. This concept concerns mixtures of hydrogen bonded liquids, where the difference in local kinetics of different species lead to the appearance of long lived local structures, organized through hydrogen bonding, which we describe in terms of charge ordering kinetics. However, the present work concerns single component liquids, and is meant to build the bases for each species, in view to study mixtures in subsequent works, under the perspective of the duality of fluctuation micro-structure.

The remainder of the paper is organized as follows. In the Section 2 we review the charge ordering concept in order to clarify what is exactly meant by this wording in the context of our approach. In section 3 the technical details about simulation and theoretical background are presented. Our results for different types of liquids are shown in the results section 4. Finally we present a discussion and our conclusion in section 5.

2 Model, simulation and theoretical details

All systems contain a total of 2048 molecules. GROMACS program package [48, 49] was used for all of the simulations. Packmol software [50] was utilized to obtain initial configurations. Total equilibration in both NVT and NPT ensembles was performed for 1 ns, after which an NPT production run of 1 ns was used to calculate all statistical quantities. The temperature was kept at T=300 K by using the Nose-Hoover thermostat [51, 52] with the time constant of 0.1 ps. The pressure was fixed at p=1 atm with the Parinello-Rahman barostat [53, 54] with the time constant of 1 ps. Leap-frog integration [55] with time step of 1 fs was used to generate trajectories and constraints were handled with the LINCS algorithm [56]. The cut-off radius for short-range interactions was 1.5 nm. Long-range Coulomb interactions were handled with the particle mesh Ewald (PME) method [57], with FFT grid spacing of 0.12 nm and interpolation order of 4. Force fields are SPC/E [58] for water and OPLS-UA [59] for alcohols.

Static cluster distributions can be obtained directly from the Gromacs auxiliary programs[24]. In the present paper, however, we are interested in the clusters as they appear in the pair correlation function, mainly through the cluster peak in the intermediate scattering function $F(k,t)$. Our approach is discussed in Section 4.2.

The dynamical atom-atom correlation functions are computed from simulations. In general, it is found that all dynamical functions are significantly decayed within 100ps. The calculated functions are as follows. If $\rho_{a_i}(\mathbf{r},t) = \delta(\mathbf{r}-\mathbf{r}_{i_a}(t))$ designates the time dependent local density of atom "a" of a molecule "i" in the liquid, located at position $\mathbf{r}$ at time t, then from this random variable on could define another random variable which is the total dynamical density of atom "a" as $\rho_a(\mathbf{r},t) = \sum_{i=1,N} \rho_{i_a}(\mathbf{r},t)$, where N is the number of molecules. From these 2 random variables, using the isotropy and homogeneity of the liquid state, one can define the total van Hove dynamical correlation function between a pair of atoms "a" and "b" as [10] by the ensemble average

$$G_{ab}^{(t)}(r,t) = \frac{1}{N\rho} < \rho_a(\mathbf{r},t)\rho_b(\mathbf{r}=\mathbf{0},t=0> \tag{1}$$

which is decomposed in self and distinct atom contributions

$$G_{ab}^{(t)}(r,t) = G_{ab}^{(s)}(r,t) + G_{ab}^{(d)}(r,t) \tag{2}$$

We note that the self van Hove function is the dynamical analog of the W-matrix element in the RISM (Reference Interaction Site Model) [60, 61, 62], and represents in fact the intra-molecular correlations between two atoms, while $G_{ab}^{(d)}(r,t)$ is the dynamical equivalent of the static pair correlation function, to which it reduces at $t = 0$:

$$G_{ab}^{(d)}(r,t=0) = g_{ab}(r) \tag{3}$$

Note that the van Hove function is normalized by the density such that this equality holds.

The r-Fourier transform gives the intermediate scattering function $F(k,t)$ defined as:

$$F_{ab}^{(t)}(k,t) = \int d\mathbf{r} G_{ab}^{(t)}(r,t)\exp(i\mathbf{k}.\mathbf{r}) = F_{ab}^{(s)}(k,t) + F_{ab}^{(d)}(k,t) \tag{4}$$

and equally separated in self and distinct parts. We note that at $t = 0$, $F_{ab}^{(t)}(k,t=0) = S_{ab}(k)$,which is the total static structure factor defined by $S_{ab}(k) = W_{ab}(k)+\rho\int d\mathbf{r}\,[g_{ab}(r)-1]\exp(i\mathbf{k}.\mathbf{r})$, where $W_{ab}(k)$ is the intra-molecular correlation function, which then corresponds to the self-part of the van Hove function.

Herein, we shall focus on the distinct correlation functions which are better suited to understand how different molecules correlate and cluster between themselves under Coulomb interactions. Details on various dynamical correlation functions will be reported in a subsequent paper.

The last point corresponds to the relation between peak positions k_p in the structure factors $S_{ab}(k)$ and the corresponding distance r_p in the pair correlation functions $g_{ab}(r)$. The typical Fourier transform relation is

$$r_p k_p \approx 2\pi \tag{5}$$

While the peak k_p are often well defined, it is the interpretation of the distance r_p which is ambiguous. In many cases, this distance $r_p \approx 2\pi/k_p$ is associated to the mean intermolecular distance, wrongly so from our point of view. We provide here a demonstration of this statement. We note that this interpretation, when associated to the main peak of the structure factor, often in the range $1.5\mathring{A}^{-1} < k_p < 2\mathring{A}^{-1}$, corresponds to distances $3\mathring{A} < r_p < 4.5\mathring{A}$, which cover typical atom sizes, and, therefore correspond to the main peak in $g_{ab}(r)$. In dense liquids, molecules are so close that the mean atom-atom distance is no so much different than the mean atom size. The test between the two propositions is made when considering the low density form of $S(k)$. This can be obtained from integral equation theories, for instance for an atomic liquid. It is found that the main peak in $S(k) = 1 + \rho h(k)$, where $h(r) = g(r) - 1$, is always positioned in the same range as in the dense liquid. We note that the peak of $S(k)$ is related to that of $h(k)$. This can be extended rigorously down to the limit of zero density $\rho = 0$. In this case, one has exactly $g(r) = \exp(-v(r)/k_BT) + 1 = f_M(r)$, the latter which is the Mayer function $f_M(r)$. Accordingly, the main peak of $f_M(r)$ corresponds to the minimum of the pair interaction $v(r)$, which in turns corresponds to the mean atom-atom contact $r_p \approx \sigma_{ab}$. Using the Lorentz rule, we find that $\sigma_a = (\sigma_a+\sigma_b)/2$, which in the particular case of the same atom, does indeed correspond to the atom size σ_a, and not the atom-atom mean distance in the dilute gas phase. Therefore, we will safely use the correspondence in Eq.5 throughout the present work.

3 Charge order through pair correlations

Charge order is an important structuring feature in disordered liquids [10, 3, 5, 6].Since molecular interactions in liquids are essentially governed by neutral Lennard-Jones (LJ) interactions and Coulomb interactions, the quality of the disorder induced by these two types of interactions. Pair correlation functions and associated structure factors allow to illustrate the special form of order. In all classical force fields used in the literature, the pair interaction $v(1,2)$ between 2 molecules 1 and 2 is given as as sum of the (12,6) Lennard-Jones and Coulomb components between each pair of atoms i belonging to molecule 1 and j to molecule 2, separated by inter-atom distance r:

$$v(1,2) = \sum_{i_1,i_2} \left\{ 4\epsilon_{ij} \left[\left(\frac{\sigma_{ij}}{r}\right)^{12} - \left(\frac{\sigma_{ij}}{r}\right)^{6} \right] + L_B \frac{Z_i Z_j}{r} \right\} \tag{6}$$

with the usual Lorentz-Berthelot convention $\sigma_{ij} = (\sigma_i + \sigma_j)/2$ and $\epsilon_{ij} = \sqrt{\epsilon_i \epsilon_j}$, Zi is the valence of atom i and $L_B = e^2/4\pi\epsilon_0$, where e is the elementary charge and ϵ_0 the dielectric permittivity of vacuum.

3.1 Charge order in atomic model ionic liquid

To illustrate the differences between correlations, we first examine charge order in simple atomic liquids and molten salts, as illustrated in Fig. 1. The left panel

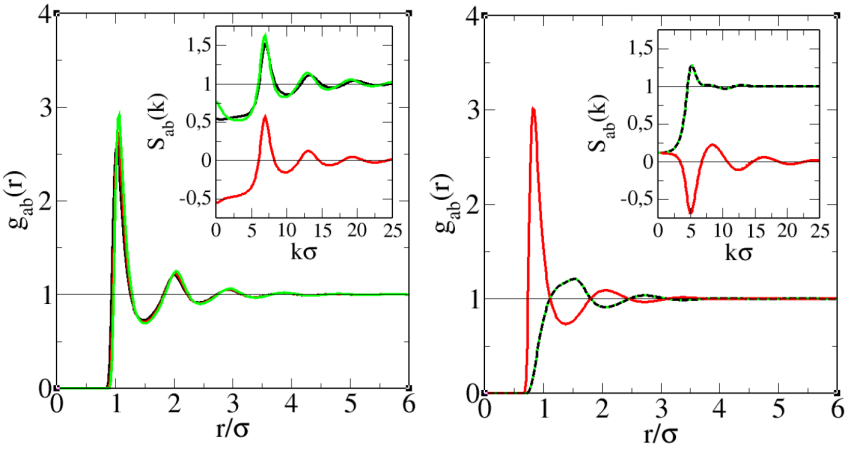

Figure 1: Illustration of charge order through correlation functions. Left panel: Lennard-Jones binary mixture. Right panel: ionic liquid. Line symbols: g_{11} in black, g_{12} in red and g_{22} in green dashes. The insets show the structure factors with same color conventions.

shows typical binary LJ correlation functions between atoms a and b and , as well as the corresponding structure factors (inset), defined as

$$S_{ab}(k) = \delta_{ab} + \rho\sqrt{x_a x_b}\int d\mathbf{r}\,[g_{ab}(r) - 1]\exp(i\mathbf{k}.\mathbf{r}) \tag{7}$$

The following parameters are used. All particles diameters are the same $\sigma_{11} = \sigma_{12} = \sigma_{22} = 3\mathring{A}$. The LJ energy parameters are $\epsilon_{11}/k_B = 100$K, $\epsilon_{11}/k_B = 150$K , $\epsilon_{11}/k_B = 200$K . The number density is $\rho = 0.684$ (molar volume is $V_m = 17.75\text{cm}^3$ /mol) and the temperature $T = 100$K. Equimolar case $x_1 = x_2 = 0.5$ is considered.

The right panel shows typical ionic salt with following parameters. The diameters are as above with $\sigma_{ij} = 3\mathring{A}$. The valences are $z_1 = 1$ and $z_2 = -1$. The dispersion interactions are limited to the repulsive part of the LJ interaction, with $\epsilon/k_B = 50$K. The number density is $\rho = 0.9$ and the temperature $T = 2000$K.

On the left panel, all the pair correlation functions $g_{ab}(r)$ are seen to be in phase. This case can be considered as a particular case of ionic liquid with zero valence $z = 0$. In particular the peaks of the structure factors are all positive. The right panel illustrates charge order in a disordered ionic liquid. One notices the typical signature of charge order, such as dephasing between the like correlations $g_{++}(r) = g_{--}(r)$ and the cross charge correlations $g_{+-}(r)$, and their consequence for the structure factor with a positive and negative peak at $k = 2\pi/d_{\text{contact}}$, with $d_{\text{contact}} < \sigma$ ($d_{\text{contact}}/\sigma < 1$) as seen in main peak of $g_{+-}(r)$ $S_{+-}(k)$ at. As a consequence of this dephasing, the like structure

factor $S_{++}(k) = S_{--}(k)$ are seen to have a negative anti-peak, at the same position as the positive peak of $S_{+-}(k)$ at $k\sigma = 5 < 2\pi$. This corresponds to a large distance $r \approx 1.2\sigma$, which corresponds approximately to the +- dimer-dimer closest distance.

Charge order for complex ionic liquids, and particularly room temperature ionic liquids, and in relation to molecular structural positioning through pair correlation functions and structure factors, has been discussed by several authors [7, 9, 14, 5].

3.2 Charge order in polar hydrogen bonding molecular models

In the case of molecular models, atoms, charged or not, are tied inside molecules, and there is a local competition between charge order and ordinary disorder produced by the LJ part of the pair interaction. This competition imposes the molecules to rotate in order to properly position themselves next to another molecule. This induces a positional competition, with non-unique solutions and frustration issues, and which differs for different types of molecules. Since charge order is the most apparent in highly polar molecules, such as water and alcohol, for example, we examine below the case of water, methanol and ethanol. In addition to this competition, there is the issue that if the molecules were cut into separate pieces containing the pure LJ part and pure Coulomb part, then the mixture will phase separate since both types of interactions are incompatible with each other. This means that the relative concentration fluctuation will play a capital role in this process of phase separation. This process is not allowed when both pieces are tied into a single molecule. Hence, the density and concentration fluctuation of the molecules will still continue to play an important role through the way they will position next to each other. The concept of the duality of concentration fluctuation and charge order characterizes this feature.

3.2.1 Water

In the case of water, all 3 sites (2 hydrogen (+0.424) and 1 oxygen (-0.848)) are charged, and charge order is driven only OO, OH and HH Coulomb interactions. Fig. 2 below shows the corresponding pair correlation functions (left panel) and structure factors (right panel). Note that the OH structure factor is shifted upward by 1, when compared with Fig. 1.

We immediately note the charge order with the phase opposition between $g_{OH}(r)$(red curve) and $g_{HH}(r)$(green curve). However, charge order with opposing peaks is seen in the structure factor at $k = 3\mathring{A}^{-1}$, which is the second peak, and not the first, as in Fig.1(right panel). Indeed, the corresponding distance is $r = 2$ Å, which exactly the hydrogen bonding distance between the O and H sites of different molecules, but which appears simply as the consequence of charge order. The 'main' peak at $k = 2\mathring{A}^{-1}$ is in fact corresponding $r = 3$ Å, which is the water-water contact, hence corresponds to the second physical distance in the liquid.

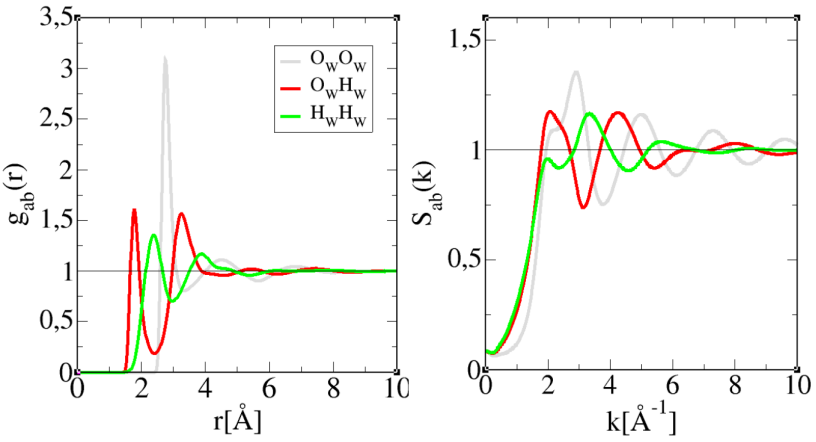

Figure 2: Charge order for water pair correlation functions (left) and structure factors (right). The lines color are as in the inset.

The O-O correlation are grayed-out because they do not fit the charge order criteria, as in Fig. 1, where it should correspond to the behaviour of the black curve. Instead, the $g_{OO}(r)$ appears difficult to interpret in terms of charge order. However, the structure factor $S_{OO}(r)$ regroups nicely the 2 distances in the well known split peak, the first at $k = 2\AA^{-1}$ and the second at $k = 3\AA^{-1}$, corresponding respectively to the water-water contact and hydrogen bonding distance. In fact, these 2 distances also appear in the $g_{OO}(r)$: the first peak is positioned at the water-water contact (which is more 2.8 Å than 3 Å), while the periodicity of the oscillations is 2 Å. This discussion illustrates the possibility to reinterpret water correlations in terms of charge order alone. In particular, the discussions about the water-water Hbond alignment [63], corresponding tetrahedrality [64, 65] and possibility of a 5th neighbour [66, 67, 68], become byproducts of the charge ordering.

3.2.2 Methanol

Fig.3 shows the pair correlation functions (main panel) and structure factors (inset) for the 2 most important charged sites, oxygen O (-0.674) and hydrogen H (+0.408). The methyl site CH3 (+0.266) is weakly charged and does not show features as prominent as the first two. Indeed, it has been demonstrated in our previous work [5, 6] that charge ordering is relevant only for partial charges above valence Z=0.4.

The features observed bear many resemblances to those of water. Only the OH and HH pair correlation show typical phase opposing oscillations. The corresponding structure factors show the typical positive and negative peaks at $k = 3\AA^{-1}$, which is the Hbonding distance r=2Å, just like water. This is also the period of oscillations for all the $g(r)$. The oxygen-oxygen contact peak at

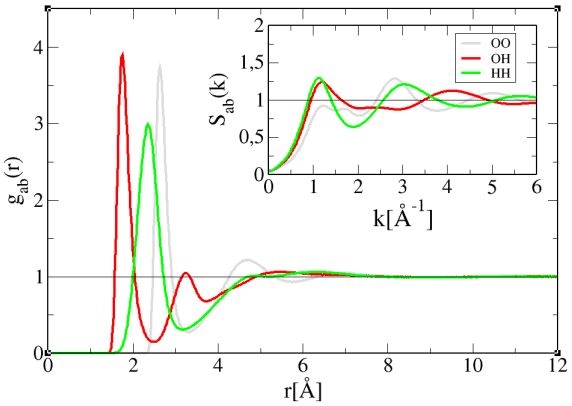

Figure 3: Charge order for methanol pair correlation functions and structure. The lines colors are as in the inset.

$k = 2\mathring{A}^{-1}$ ($r = 3\mathring{A}$) is barely visible, except on the OH correlations, but, instead a prominent pre-peak is seen at $k \approx 1\mathring{A}^{-1}$, which is common to all structure factors, indicating that all pair correlations are equally affected. It corresponds larger oscillatory modes in $g(r)$, seen by the peak around 8 Å, which characterizes the existence of Hbonded aggregates. We previously interpreted this feature [6] in terms of depletion correlations beyond r=3 Å, which correspond to chain formation of the OH hydroxyl groups, hence depleting the number of OH from a more uniform distribution.

3.2.3 Ethanol

Fig. 4 shows the pair correlations (main panel) and structure factors (inset) for ethanol, the same way it was done for methanol above in Fig.3. In the OPLS model, the oxygen, hydrogen and first methylene sites, bear the same partial charges as for methanol. Similarly to methanol, the carbon bases sites are not affected by charge order correlation, since their charges are too low (below $Z = 0.4$). For the OPLS model, the partial charge of the methyl site is zero.

The features observed bear many resemblances to those of water and methanol. Only the OH and HH pair correlation show typical phase opposing oscillations. The oxygen-oxygen contact peak at $k = 2\mathring{A}^{-1}$ ($r = 3\mathring{A}$) is barely visible, except on the OH correlations, but, instead a prominent pre-peak is seen at $k = 0.76\mathring{A}^{-1}$, which is common to all structure factors, indicating that all pair correlations are equally affected. It corresponds larger oscillatory modes, see by the depletion correlations after the first $g(r)$ peak, and the mid-range peak around 8 Å, which characterizes the existence of Hbonded aggregates.

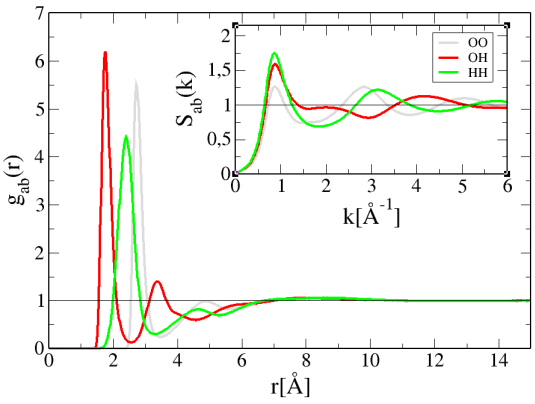

Figure 4: Charge order for ethanol pair correlation functions and structure. The lines colors are as in the inset.

4 Results

Aside being hydrogen bonding liquids, water and alcohols are not usually discussed comparatively in the literature and textbooks, since their physico-chemical properties are very different [69]. This difference can be primarily attributed to the fact that alcohol molecules have neutral CH groups attached the OH hydroxyl head group, while water has none. Yet, the analysis of static correlation functions and clusters show many analogies, all of which stem from the charge ordering induced by the OH chaining. This is the starting point of our analysis, deliberately ignoring differences in macroscopic properties, and in search of a common explanatory ground at microscopic level. As a basis for a counter argument, it is noteworthy that the partial charges on the oxygen and hydrogen atoms differ between the water and alcohol models.

4.1 Analysis of static correlation functions

Fig. 5 shows the striking similarities between the OO and OH correlations for all 3 liquids: marked first peaks centered at the OO and OH contacts. The fact that the OO contact is higher than the OH contact goes against the simple charge order as seen in Fig. 1 for unbound charges. However, it is fully compatible with an O-H..O alignment correlation, which is also the signature of Hbonding correlations. A notable difference for the OO correlations between water and alcohols is the pronounced depletion at second and third neighbour correlations, which is a signature of chain-like OH group clusters. As discussed previously, it is the combination of high OO peak and neighbour depletion which produce the scattering pre-peak, and the absence of depletion correlations for water could explain the absence of pre-peak.

Indeed, Fig. 6 shows the structure factors corresponding to functions shown

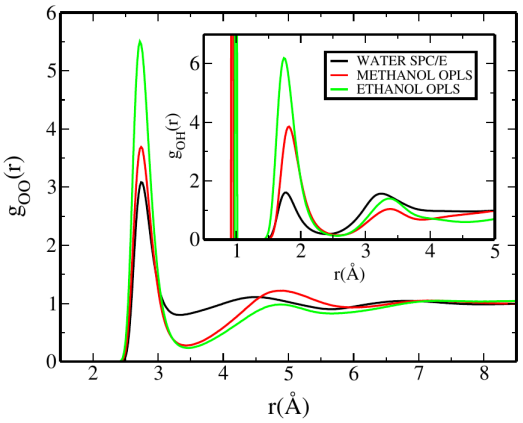

Figure 5: Main panel: $g_{OO}(r)$ (inset $g_{OH}(r)$) for SPC/E water (black), OPLS methanol (red) and OPLS ethanol (green)

in Fig. 5, and the pre-peaks are quite apparent for methanol and ethanol $S_{OO}(k)$, as signaled by the vertical lines. Since these k-peaks correspond to the main peaks in $S_{OH}(k)$ functions (inset), we conclude that they concern the collective Hbond, hence the cluster peaks. However, two intriguing features are seen, which has not been noticed previously, to our knowledge. The first concerns the $S_{OO}(k)$ peaks marked with gray arrows, at $k_C \approx 1.7\mathring{A}^{-1}$, well marked for methanol, but less apparent ethanol, more like a flattening. This k-value corresponds to the distance $r_C \approx 2\pi/k_C \approx 3.5\mathring{A}$, which is quite close to the diameter of the oxygen atom in the OPLS models $\sigma_O \approx 3.1\mathring{A}$, and corresponds to the first minimum of all the $g_{OO}(r)$ function in Fig.5. In other words, this peak corresponds to a direct first neighbour OO correlation.

The second feature is in fact the common peak for all 3 liquids, found for $S_{OO}(k)$ at $k \approx 3\mathring{A}^{-1}$, and which would correspond to a distance $r \approx 2\mathring{A}$, which is too small to represent any relative positions of the oxygen atoms whose size is close to $3\mathring{A}$. In fact, this peak is a consequence of the OH charge ordering oscillations in the following way. It corresponds to the Hbonding distance of $2\mathring{A}$ between an oxygen in the first neighbour and another oxygen in the second neighbour layer, as can be seen in Fig.4. In other words, this is a 3-body effect as seen from the pair correlations in Fig.4. The consequence of these two features, is that, when applied to $S_{OO}(k)$ of water, it demonstrates that the shoulder peak around $k \approx 2\mathring{A}^{-1}$ is in fact the OO contact peak, while the more apparent peak at $k \approx 3\mathring{A}^{-1}$ does not correspond to any relative oxygen atom positions, just like for the alcohols. But there is more, the main peak for water $S_{OH}(k)$ is equally positioned at $k \approx 2\mathring{A}^{-1}$, suggesting an unphysical OH contact at $r \approx 3\mathring{A}$, since it is too large than the expected $r_{OH} \approx 2\mathring{A}$. By analogy with the alcohols, it suggests that it could be a water "pre-peak" position, hence implying that the shoulder peak of $S_{OO}(k)$ is both the OO contact peak and pre-peak,

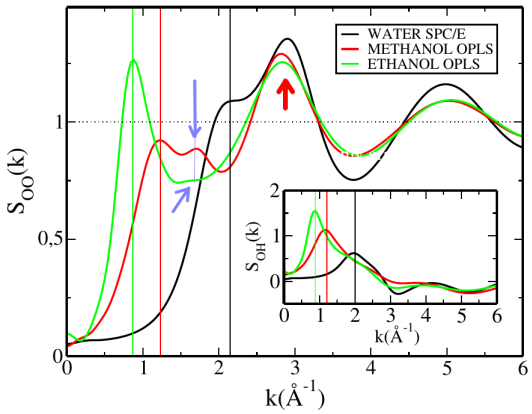

Figure 6: Main panel: $S_{OO}(k)$(inset $S_{OH}(k)$). Color codes as in Fig. 5 The gray arrows mark the k-vector associated to the atom-atom contact peak; the vertical lines mark the cluster pre-peak typical of the alcohols, which are better distinguished in the $S_{OK}(k)$ in the inset. The thick red arrow shows the charge order peak, which is found to be the *same* for all 3 molecules - thus illustrating the main point of this paper.

which is a feature never suggested in the past literature of water.

The intriguing results of the analysis above require a better investigation in order to confirm them, which is provided by the analysis of the dynamical correlations below, hence providing the missing link between the static picture and the kinetics of labile Hbonded aggregates. We also note that none of the discussions so far required considering explicitly the O-H..O hydrogen bonding criteria in a direct manner, and consequently, charge ordering criteria alone is sufficient so far.

4.2 Analysis of dynamical correlation functions

Since we are interested in hydrogen bonding correlations between different molecules, we focus herein solely on the analysis of the oxygen-oxygen correlation functions, both in r and k space, and analyse the decays of the major peaks in relation to the local microstructure.

4.2.1 van Hove and intermediate scattering functions

Fig.7. shows the oxygen-oxygen total van Hove function $G^{(t)}_{O_W O_W}(r,t)$ for SPC/E water as well and the corresponding intermediate scattering function $F^{(t)}_{O_W O_W}(k,t)$, for different times. The major features in r-space are the rate of decays of the self part at $r = 0$, and the main peak at $r \approx 3\mathring{A}$, the latter which is discussed in Fig.10 below. The major feature in k-space is that the decay of the cluster

peak at $k \approx 2\mathring{A}^{-1}$ is slower than that of the Hbond peak at $k \approx 3\mathring{A}^{-1}$. This is discussed in Fig.11 below.

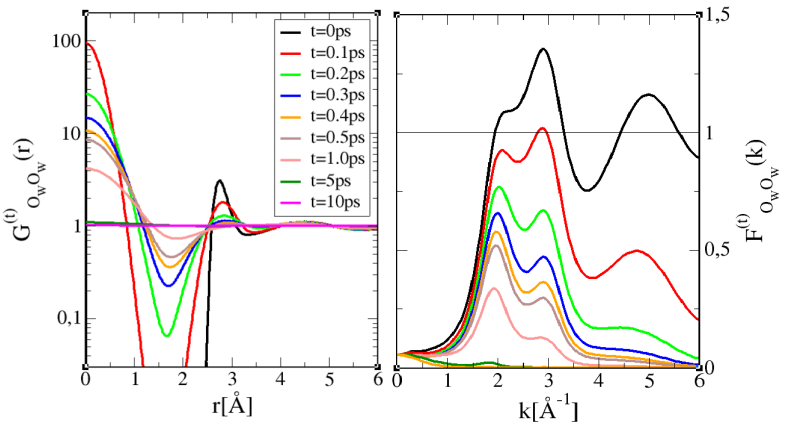

Figure 7: Dynamical correlation functions for SPC/E water. Left panel, total van Hove function for oxygen atom correlations $G_{OO}^{(t)}(r,t)$ (in log-scale) for different times, as shown in the legend panel. Right panel, corresponding intermediate scattering functions $F_{OO}^{(t)}(k,t)$.

A similar analysis can be conducted for methanol in Fig.3 and ethanol in Fig.4. Unlike water, for these alcohols the Hbond cluster peak (pre-peak) is well separated from the contact peak at $k \approx 2\mathring{A}$.

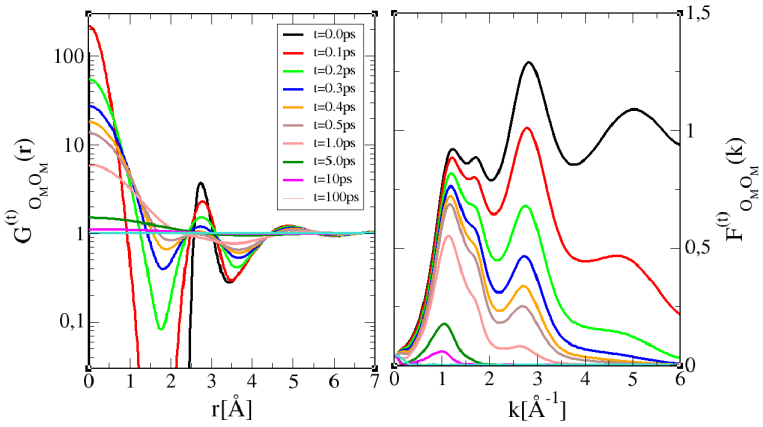

Figure 8: Dynamical correlation functions for OPLS methanol. Leftt panel, total van Hove function for oxygen atom correlations $G_{OO}^{(t)}(r,t)$ for different times, as shown in the legend panel. Right panel, corresponding intermediate scattering functions $F_{OO}^{(t)}(k,t)$. The blue arrow shows the Hbond cluster pre-peak.

These 3 figures show how the cluster pre-peak detaches clearly and becomes prominent, when going from water to ethanol.

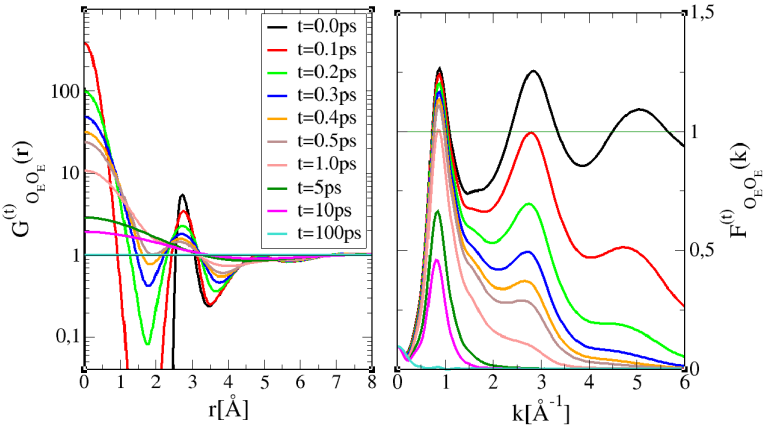

Figure 9: Dynamical correlation functions for OPLS ethanol. Leftt panel, total van Hove function for oxygen atom correlations $G_{OO}^{(t)}(r,t)$ for different times, as shown in the legend panel. Right panel, corresponding intermediate scattering functions $F_{OO}^{(t)}(k,t)$. The blue arrow shows the Hbond cluster pre-peak.

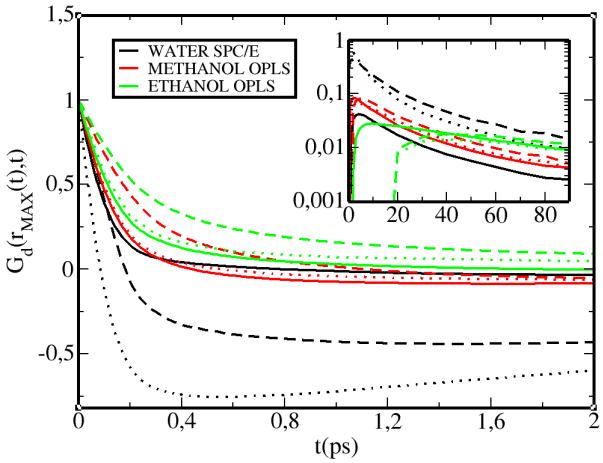

Figure 10: Time dependence of distinct van Hove function $G_{AB}^{(d)}(r_{AB},t)$ at the atom$_A$-atom$_B$ contact distance r_{AB} corresponding to the main peaks in Fig.1 for each type of the 3 liquids. The inset shows the long time decay in log scale. Color conventions as Fig. 5 Full lines for AB=OO, dotted lines for AB=OH and dashed lines for AB=HH.

4.2.2 Analysis of the decay of dynamical correlations

We analyse in more detail the dynamical decays of the r and k typical peaks of the oxygen-oxygen correlation functions.

The main panel of Fig. 10 shows the decay of the OO and OH main peaks of the pair correlation functions of Fig. 5, in the range of 0-2 ps, while the inset focuses on the long time scale (with vertical log scale). The first feature which is immediately apparent is the hierarchy of time decays, the fastest for water and slowest for ethanol, with a narrower difference between the 2 alcohols. This feature alone indicates that the temporal decay of charged atom correlations is vastly different for water and the 2 alcohols, despite the static correlations presenting appealing similarities. The second feature is that time decays between the various atom-atom correlation show more difference between themselves for water than for the alcohols, indicating that the charged group motions are more "homogeneous" for alcohols than for water. Going into specific details, for water, the OH decay is the fastest, while the OO decay is the slowest, which seems contradictory: if the OH contact decorrelates very fast, then the auxiliary OO contact should also decay accordingly. The only way to reconcile these contradictory decays is that the rotation of the OH arm is such that it re-establish the OO contact. This is precisely the jump rotation motion advertised in recent investigations [70, 71, 72], and is found to be contained in the dynamics of a classical model of water. For alcohols, it is the opposite which is found, namely that the OO decay is faster than the OH decay, denoting that the hydrogen bonding holds the hydroxyl group clusters.

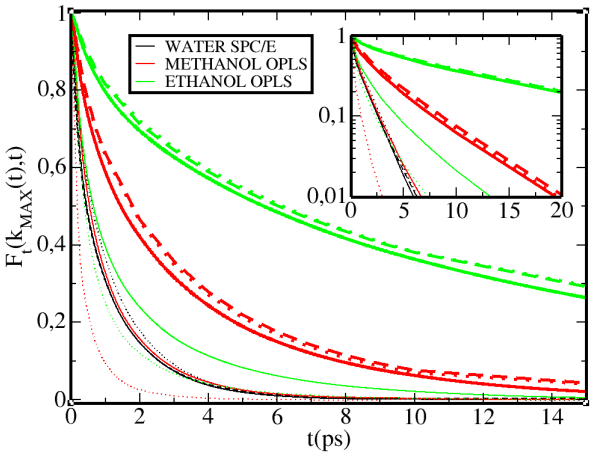

Figure 11: Time dependence of total intermediate scattering function $F_{AB}^{(t)}(k_P, t)$, for the various peaks signaled in Fig. 6 by the vertical lines positioned at the different k_P values, and discussed in the text. The pre-peaks are shown in thick lines and the main peaks in thinner lines. The line styles follow the same atom-atom conventions as in Fig. 6. The inset shows the same information but in log scale (see text).

The long time decay shown in the inset suggests a near exponential behaviour, as expected for equilibrium liquids with simple diffusion, and a perfect isotropy for all atoms. It is seen that water and methanol have a similar decay, while ethanol has a markedly slower decay, suggesting slower global dynamics, which is also compatible with the higher viscosity of this liquid.

Fig. 11 shows the time decays of the various peak positions we discussed in Fig. 6, through the total intermediate scattering function $F_t(k, t)$, and the inset shows the log scale version, to underline the quasi-exponential decays. While the dynamics in r-space is directly intuitive as referring to actual atom motions, that in k-space is more difficult to grasp, since k-peaks reflect global trends.

Let us first discuss the 2 alcohols (in red for methanol and green for ethanol). Two types of curves should be distinguished in Fig. 11, that for the alcohol pre-peaks in thick lines, and that for main peaks in thinner lines. These correspond to cluster dynamics and contact dynamics, respectively. In comparison with Fig. 10, the time decay in k-space shows much more marked differences between different types, which indicates an important difference with water, as discussed later below.

The pre-peaks are seen to decay slower for ethanol than for methanol, and moreover, all atom-atom curves are almost superposed. Both results are quite expected: cluster dynamics in ethanol is intuitively expected to be slower than that of methanol, because of the additional methyl group. The near superposition of all 3 atom-atom curves indicate that the global motion are quite similar,

with the OO decay slightly faster than the others. This result suggests that it is really the charge order which drives cluster dynamics. The thinner curves concern global atom-atom contact dynamics, and, as far as species are concern, they follow the same pattern, namely slower for ethanol than for methanol. However, within each species, they differ from the pre-peak behaviour since the atom-atom contact decays are different. For alcohols, the OO decay is slower than the OH decay, which is the exact opposite of what we found for the cluster peak dynamics. It suggests that the spatial frequency of the OO and OH motions at contact decays faster than the same atoms in clusters. We believe that this is an important result concerning liquids that have specific cluster peaks in radiation scattering experiment, and that this difference is related to a more global kinetic of clusters, as opposed to the dynamics of individual atoms within the clusters. Namely, this global dynamics is very different between different atoms, while being the same when considering the same atoms, but within a cluster.

Concerning water, the most apparent feature is that the behaviour in k-space looks just the opposite of that in r-space seen in Fig. 10. Namely that there is more dispersion for the alcohols between the various atom-atom correlations, while that of water are superposed. In other words, in k-space, it is water which looks more "homogeneous" than alcohol, the exact opposite of what we found in r-space. Seen from a k-space perspective, water appears as more "isotropic" and "homogeneous". We believe that it is precisely at the origin of the contradicting dual pictures of water, both as a structured liquid [73, 74, 65] and as an ordinary liquid of small molecules [34, 35, 75]. The first picture could account for the rich microscopic dynamics of water in the real space [64, 76, 77, 78], while the second picture could refer to the almost disappointingly "simple" dynamics of all atom-atoms decays in k-space [79, 36]. The present analysis provides both a microscopic support for the two interpretations and an explanation for the apparent contradiction. In view of the related controversies in the past, the present analysis provides a resolution of an old problem.

4.3 Dynamics of clusters

The mean life time of clusters can be obtained by fitting the long time decay of the cluster peaks τ in k-space in Fig.11 by an exponential form exp(-t/τ), which fits very well as can be seen from the inset. The decay time τ can be interpreted as a mean cluster lifetime. For water, we obtain a very short time of $\tau \approx 1.45$ps, for methanol $\tau \approx 4.5$ps and for ethanol $\tau \approx 18$ps.

It is instructive to examine the pictorial confirmation of some of the features discussed previously. The direct static oxygen atoms cluster calculation, as in our previous work [21, 22, 24] can be made with the oxygen-oxygen distance cutoff to be $3.5\mathring{A}$, which is the first minimum of the $g_{OO}(r)$ functions. For the alcohols, it was found that there is a cluster mean size for 5-7 molecules (see for instance Fig.7 in Ref.[24]). For water, there is no such marked peak[21, 22].

Alternatively, for a given cluster of mean size, its dynamics can be followed through the VMD code, and mean lifetime of a cluster is evaluated visually.

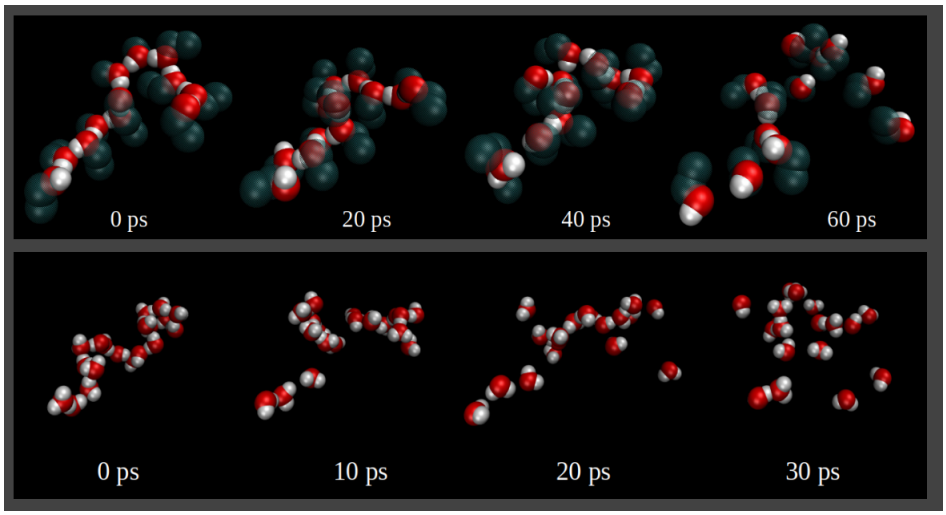

Figure 12: Evolution in time of the cluster dynamics for ethanol (top) and water (bottom). The time is indicated on each frame.

For alcohols, it is empirically observed that, for large clusters, they often break down to mean size clusters of 5-7 monomers, consistent with static calculations, and the final lifetime is controlled by these. This explains the main peak in the cluster distribution. For water, since there is no mean cluster peak, the life time is rather short, about 1.5ps.

Fig.12 shows a few frames of the internal dynamics of typical clusters, for ethanol and water. The corresponding movies can be found in the SI material accompanying this paper. What is apparent is that the ethanol clusters live longer than that of water. From this particular example, ethanol cluster mean lifetime is about 20ps, as illustrated in Fig.12, while that of water less than 10ps. This is precisely at the origin of the radiation scattering pre-peak: since the global structure is long lived, the corresponding atom-atom correlations are saved into the correlation functions, hence producing the high first peak and depletion secondary peaks typical of alcohol OO correlations. For water, although the clusters are similar, those are destroyed much faster into smaller dimer-like shapes. Although these might be part of other clusters, the internal coherence of the initial cluster is lost. This implies that the chain-like correlations are not "saved" as a typical configuration into the pair correlation functions.

We believe that this is reason why there is a "phantom" cluster peak in the shoulder pre-peak of water $S_{OO}(k)$, which is could be interpreted as both a contact and a cluster peak at $k \approx 2\mathring{A}^{-1}$. The evidence of this dual interpretation of the shoulder peak of water is probably related to the dual contradictory picture of water mentioned in the previous section.

5 Discussion and Conclusion

The analysis presented herein reveals several points about the local structure of hydrogen bonded liquids as seen from a dynamical point of view. First of all, hydrogen bond order appears as a particular case of the more general charge order. It is the immediate proximity of the positive charge on the hydrogen atom and the negative charge on the oxygen atom that drive the local structure of these liquids. This is perhaps the most apparent in the striking similarities of the instantaneous cluster structures in water and in alcohols, as illustrated in Fig. 12. It explains the pronounced similarities in the static OO correlations as well as the differences in the OH correlations, as seen in Fig. 5 and Fig. 6.

However, it is the dynamical correlations which reveal the difference between the similarities in different micro-states (snapshots) and the strong differences on how the system evolves in time from one microstate to another. Our analysis shows that it is this dynamical evolution which explains several features observed previously in the literature, such as the jump rotation of the OH arm for water [70, 71, 72], or the contradictory pictures of the importance of the water structure [73, 74, 34, 36]. Perhaps the water tetrahedrality has been put too much at the center of water local structure [74, 64, 78], originating from the dual structure picture advocated by Frank [39] and his successors [40, 65, 27]. The discussion of Figs. 10 and 11 shows that dynamical correlations, both in real and reciprocal space, provide a very rich information about the dynamics, both at atomic and cluster level, almost like a movie.

We expect that this analysis of time correlation functions will help provide a better understanding of the micro-heterogeneity in mixtures of associated liquids.

Supplementary Information details

A supplementary file describing the two MP4 movies files is provided. The two movies show the evolution in time of a cluster of SPC/E water and OPLS ethanol.

Acknowledgments

This work has been supported in part by the Croatian Science Foundation under the project UIP-2017-05-1863 “Dynamics in micro-segregated systems”.

References

[1] Atkins, P.; De Paula, J. *Atkins physical chemistry*. Oxford University Press, 8th edition ed., **2006**.

[2] Hansen, J. P.; McDonald, I. R. Self-diffusion and electrical conductance in a simple molten salt. *Journal of Physics C: Solid State Physics* **1974**. *7*, L384.

[3] Hansen, J. P.; McDonald, I. R. Statistical mechanics of dense ionized matter. iv. density and charge fluctuations in a simple molten salt. *Phys. Rev. A* **1975**. *11*, 2111–2123.

[4] Del Pópolo, M. G.; Voth, G. A. On the structure and dynamics of ionic liquids. *J. Phys. Chem. B* **2004**. *108*, 1744–1752.

[5] Perera, A.; Mazighi, R. Simple and complex forms of disorder in ionic liquids. *Journal of Molecular Liquids* **2015**. *210*, 243–251. Mesoscopic structure and dynamics in ionic liquids.

[6] Perera, A. Charge ordering and scattering pre-peaks in ionic liquids and alcohols. *Phys. Chem. Chem. Phys.* **2017**. *19*, 1062–1073.

[7] Santos, C. S.; Annapureddy, H. V. R.; Murthy, N. S.; Kashyap, H. K.; Castner, E. W.; Margulis, C. J. Temperature-dependent structure of methyltributylammonium bis(trifluoromethylsulfonyl)amide: X ray scattering and simulations. *The Journal of Chemical Physics* **2011**. *134*, 064501.

[8] Siqueira, L. J. A.; Ribeiro, M. C. C. Charge ordering and intermediate range order in ammonium ionic liquids. *The Journal of Chemical Physics* **2011**. *135*, 204506.

[9] Kashyap, H. K.; Santos, C. S.; Annapureddy, H. V. R.; Murthy, N. S.; Margulis, C. J.; Castner, Jr, E. W. Temperature-dependent structure of ionic liquids: X-ray scattering and simulations. *Faraday Discuss.* **2012**. *154*, 133–143.

[10] Hansen, J.-P.; McDonald, I. *Theory of Simple Liquids*. Academic Press, Elsevier, Amsterdam, 3rd ed., **2006**.

[11] Gallo, P.; Sciortino, F.; Tartaglia, P.; Chen, S.-H. Slow dynamics of water molecules in supercooled states. *Phys. Rev. Lett.* **1996**. *76*, 2730–2733.

[12] Schulz, R.; von Hansen, Y.; Daldrop, J. O.; Kappler, J.; NoÃ©, F.; Netz, R. R. Collective hydrogen-bond rearrangement dynamics in liquid water. *J. Chem. Phys.* **2018**. *149*, 244504.

[13] Camisasca, G.; Galamba, N.; Wikfeldt, K. T.; Pettersson, L. G. M. Translational and rotational dynamics of high and low density tip4p/2005 water. *J. Chem. Phys.* **2019**. *150*, 224507.

[14] Russina, O.; Sferrazza, A.; Caminiti, R.; Triolo, A. Amphiphile meets amphiphile: Beyond the polar-apolar dualism in ionic liquid/alcohol mixtures. *J. Phys. Chem. Lett.* **2014**. *5*, 1738–1742.

[15] Tibbetts, C. A.; Wyatt, A. B.; Luther, B. M.; RappÃ©, A. K.; Krummel, A. T. Dicyanamide anion reports on water induced local structural and dynamic heterogeneity in ionic liquid mixtures. *J. Phys. Chem. B* **2023**. *127*, 932–943.

[16] Dixit, S.; Crain, J.; Poon, W.; Finney, J.; Soper, A. Molecular segregation observed in a concentrated alcohol-water solution. *Nature* **2002**. *416*, 829–832.

[17] Guo, J.-H.; Luo, Y.; Augustsson, A.; Kashtanov, S.; Rubensson, J.-E.; Shuh, D. K.; Ågren, H.; Nordgren, J. Molecular structure of alcohol-water mixtures. *Phys. Rev. Lett.* **2003**. *91*, 157401.

[18] Gupta, R.; Patey, G. N. Aggregation in dilute aqueous tert-butyl alcohol solutions: Insights from large-scale simulations. *The Journal of Chemical Physics* **2012**. *137*, 034509.

[19] Ohmine, I. Liquid water dynamics: Collective motions, fluctuation, and relaxation. *J. Phys. Chem.* **1995**. *99*, 6767–6776.

[20] Asenbaum, A.; Pruner, C.; Wilhelm, E.; Mijaković, M.; Zoranić, L.; Sokolić, F.; Kezić, B.; Perera, A. Structural changes in ethanol-water mixtures: Ultrasonics, brillouin scattering and molecular dynamics studies. *Vibrational Spectroscopy* **2012**. *60*, 102.

[21] Požar, M.; Seguier, J.-B.; Guerche, J.; Mazighi, R.; Zoranić, L.; Mijaković, M.; Kežić-Lovrinčević, B.; Sokolić, F.; Perera, A. Simple and complex disorder in binary mixtures with benzene as a common solvent. *Physical Chemistry Chemical Physics* **2015**. *17*, 9885.

[22] Požar, M.; Lovrinčević, B.; Zoranić, L.; Primorac, T.; Sokolić, F.; Perera, A. Micro-heterogeneity versus clustering in binary mixtures of ethanol with water or alkanes. *Physical Chemistry Chemical Physics* **2016**. *18*, 23971–23979.

[23] Tomšič, M.; Jamnik, A.; Fritz-Popovski, G.; Glatter, O.; Vlček, L. Structural properties of pure simple alcohols from ethanol, propanol, butanol, pentanol, to hexanol: Comparing monte carlo simulations with experimental saxs data. *The Journal of Physical Chemistry B* **2007**. *111*, 1738–1751.

[24] Požar, M.; Bolle, J.; Sternemann, C.; Perera, A. On the x-ray scattering pre-peak of linear mono-ols and the related microstructure from computer simulations. *J. Phys. Chem. B* **2020**. *124*, 8358–8371.

[25] Stanley, H. E.; Kumar, P.; Franzese, G.; Xu, L.; Yan, Z.; Mazza, M. G.; Buldyrev, S. V.; Chen, S.-H.; Mallamace, F. Liquid polyamorphism: Possible relation to the anomalous behaviour of water. *The European Physical Journal Special Topics* **2008**. *161*, 1–17.

[26] Nilsson, A.; Pettersson, L. G. M. The structural origin of anomalous properties of liquid water. *Nature Communications* **2015**. *6*, 8998.

[27] Gallo, P.; Amann-Winkel, K.; Angell, C. A.; Anisimov, M. A.; Caupin, F.; Chakravarty, C.; Lascaris, E.; Loerting, T.; Panagiotopoulos, A. Z.; Russo, J.; et al. Water: A tale of two liquids. *Chemical Reviews* **2016**. *116*, 7463–7500. PMID: 27380438.

[28] Poole, P. H.; Sciortino, F.; Essmann, U.; Stanley, H. E. Phase behaviour of metastable water. *Nature* **1992**. *360*, 324–328.

[29] Xu, L.; Kumar, P.; Buldyrev, S. V.; Chen, S.-H.; Poole, P. H.; Sciortino, F.; Stanley, H. E. Relation between the widom line and the dynamic crossover in systems with a liquid-liquid phase transition. *Proceedings of the National Academy of Sciences* **2005**. *102*, 16558–16562.

[30] Limmer, D. T.; Chandler, D. The putative liquid-liquid transition is a liquid-solid transition in atomistic models of water. *J. Chem. Phys.* **2011**. *135*, 134503.

[31] Neophytou, A.; Chakrabarti, D.; Sciortino, F. Topological nature of the liquid-liquid phase transition in tetrahedral liquids. *Nature Physics* **2022**. *18*, 1248–1253.

[32] Shi, R.; Tanaka, H. The anomalies and criticality of liquid water. *Proceedings of the National Academy of Sciences* **2020**. *117*, 26591–26599.

[33] Foffi, R.; Sciortino, F. Correlated fluctuations of structural indicators close to the liquid-liquid transition in supercooled water. *The Journal of Physical Chemistry B* **2023**. *127*, 378–386. PMID: 36538764.

[34] Pratt, L. R.; Chandler, D. Theory of the hydrophobic effect. *The Journal of Chemical Physics* **1977**. *67*, 3683–3704.

[35] Chandler, D. Interfaces and the driving force of hydrophobic assembly. *Nature* **2005**. *437*, 640–647.

[36] Graziano, G. On the cavity size distribution in water and n-hexane. *Biophysical Chemistry* **2003**. *104*, 393–405.

[37] Duboué-Dijon, E.; Fogarty, A. C.; Hynes, J. T.; Laage, D. Dynamical disorder in the dna hydration shell. *J. Am. Chem. Soc.* **2016**. *138*, 7610–7620.

[38] Röntgen, W. C. Ueber die constitution des flüssigen wassers. *Annalen der Physik* **1892**. *281*, 91–97.

[39] Frank, H. S.; Wen, W.-Y. Ion-solvent interaction. structural aspects of ion-solvent interaction in aqueous solutions: a suggested picture of water structure. *Discuss. Faraday Soc.* **1957**. *24*, 133–140.

[40] Némethy, G.; Scheraga, H. A. Structure of water and hydrophobic bonding in proteins. i. a model for the thermodynamic properties of liquid water. *The Journal of Chemical Physics* **1962**. *36*, 3382–3400.

[41] Head-Gordon, T.; Hura, G. Water structure from scattering experiments and simulation. *Chem. Rev.* **2002**. *102*, 2651–2670.

[42] Skinner, L. B.; Huang, C.; Schlesinger, D.; Pettersson, L. G. M.; Nilsson, A.; Benmore, C. J. Benchmark oxygen-oxygen pair-distribution function of ambient water from x-ray diffraction measurements with a wide q-range. *The Journal of Chemical Physics* **2013**. *138*, 074506.

[43] Rao, F.; Garrett-Roe, S.; Hamm, P. Structural inhomogeneity of water by complex network analysis. *J. Phys. Chem. B* **2010**. *114*, 15598–15604.

[44] Schlesinger, D.; Wikfeldt, K. T.; Skinner, L. B.; Benmore, C. J.; Nilsson, A.; Pettersson, L. G. M. The temperature dependence of intermediate range oxygen-oxygen correlations in liquid water. *The Journal of Chemical Physics* **2016**. *145*, 084503.

[45] Offei-Danso, A.; Hassanali, A.; Rodriguez, A. High-dimensional fluctuations in liquid water: Combining chemical intuition with unsupervised learning. *J. Chem. Theory Comput.* **2022**. *18*, 3136–3150.

[46] Perera, A. *Fluctuation Theory of Solutions*, CRC Press, chap. Concentration Fluctuations and Microheterogeneity in Aqueous Mixtures: New Developments in Analogy with Microemulsions, 190–217. **2016**.

[47] Perera, A.; Požar, M.; Lovrinčević, B. Camel back shaped kirkwood-buff integrals. *The Journal of Chemical Physics* **2022**. *156*, 124503.

[48] van der Spoel, D.; Lindahl, E.; Hess, B.; Groenhof, G.; Mark, A.; Berendsen, H. Gromacs: Fast, flexible, and free. *Journal of Computational Chemistry* **2005**. *26*, 1701.

[49] Pronk, S.; Páll, S.; Schulz, R.; Larsson, P.; Bjelkmar, P.; Apostolov, R.; Shirts, M.; Smith, J.; Kasson, P.; van der Spoel, D.; et al. Gromacs 4.5: a high-throughput and highly parallel open source molecular simulation toolkit. *Bioinformatics* **2013**. *29*, 845–854.

[50] Martínez, J.; Martínez, L. Packing optimization for automated generation of complex system's initial configurations for molecular dynamics and docking. *Journal of Computational Chemistry* **2003**. *24*, 819.

[51] Nose, S. A molecular dynamics method for simulations in the canonical ensemble. *Molecular Physics* **1984**. *52*, 255.

[52] Hoover, W. Canonical dynamics: Equilibrium phase-space distributions. *Physical Review A* **1985**. *31*, 1695.

[53] Parrinello, M.; Rahman, A. Crystal structure and pair potentials: A molecular-dynamics study. *Physical Review Letters* **1980**. *45*, 1196.

[54] Parrinello, M.; Rahman, A. Polymorphic transitions in single crystals: A new molecular dynamics method. *Journal of Applied Physics* **1981**. *52*, 7182.

[55] Hockney, R. *Methods in computational physics, vol. 9*, Orlando Academic Press, vol. 9, chap. The potential calculation and some applications, 135–221. **1970**.

[56] Hess, B.; Bekker, H.; Berendsen, H.; Fraaije, J. Lincs: A linear constraint solver for molecular simulations. *Journal of Computational Chemistry* **1997**. *18*, 1463.

[57] Darden, T.; York, D.; Pedersen, L. Particle mesh ewald: An n log(n) method for ewald sums in large systems. *The Journal of Chemical Physics* **1993**. *98*, 10089.

[58] Berendsen, H. J. C.; Grigera, J. R.; Straatsma, T. P. The missing term in effective pair potentials. *The Journal of Physical Chemistry* **1987**. *91*, 6269–6271.

[59] Jorgensen, W. Optimized intermolecular potential functions for liquid alcohols. *The Journal of Physical Chemistry* **1986**. *90*, 1276.

[60] Kovalenko, A.; Hirata, F. Self-consistent description of a metal-water interface by the kohn-sham density functional theory and the three-dimensional reference interaction site model. *The Journal of Chemical Physics* **1999**. *110*, 10095–10112.

[61] Kovalenko, A.; Hirata, F. First-principles realization of a van der waals-maxwell theory for water. *Chemical Physics Letters* **2001**. *349*, 496–502.

[62] Hirata, F. *Theory of Molecular Liquids*, Springer Netherlands, Dordrecht, 1–60. **2003**.

[63] Pauling, L. *The nature of the chemical bond.* Cornell University Press, 3rd ed., **1960**.

[64] Head-Gordon, T.; Johnson, M. E. Tetrahedral structure or chains for liquid water. *Proceedings of the National Academy of Sciences* **2006**. *103*, 7973–7977.

[65] Sciortino, F.; Geiger, A.; Stanley, H. E. Effect of defects on molecular mobility in liquid water. *Nature* **1991**. *354*, 218–221.

[66] Walrafen, G. E. Raman spectral studies of water structure. *The Journal of Chemical Physics* **1964**. *40*, 3249–3256.

[67] Walrafen, G. E. Raman spectral studies of the effects of temperature on water structure. *The Journal of Chemical Physics* **1967**. *47*, 114–126.

[68] Monosmith, W. B.; Walrafen, G. E. Temperature dependence of the raman oh-stretching overtone from liquid water. *The Journal of Chemical Physics* **1984**. *81*, 669–674.

[69] CRC Handbook. *CRC Handbook of Chemistry and Physics, 88th Edition*. CRC Press, 88 ed., **2007**.

[70] Stirnemann, G.; Laage, D. Direct evidence of angular jumps during water reorientation through two-dimensional infrared anisotropy. *J. Phys. Chem. Lett.* **2010**. *1*, 1511–1516.

[71] Laage, D.; Stirnemann, G.; Sterpone, F.; Hynes, J. T. Water jump reorientation: From theoretical prediction to experimental observation. *Acc. Chem. Res.* **2012**. *45*, 53–62.

[72] Gomez, A.; Piskulich, Z. A.; Thompson, W. H.; Laage, D. Water diffusion proceeds via a hydrogen-bond jump exchange mechanism. *J. Phys. Chem. Lett.* **2022**. *13*, 4660–4666.

[73] Frank, H. S. The structure of ordinary water. *Science* **1970**. *169*, 635–641.

[74] Stillinger, F. H. Water revisited. *Science* **1980**. *209*, 451–457.

[75] Graziano, G. Water: cavity size distribution and hydrogen bonds. *Chemical Physics Letters* **2004**. *396*, 226–231.

[76] Wernet, P.; Nordlund, D.; Bergmann, U.; Cavalleri, M.; Odelius, M.; Ogasawara, H.; Näslund, L. Ã.; Hirsch, T. K.; Ojamäe, L.; Glatzel, P.; et al. The structure of the first coordination shell in liquid water. *Science* **2004**. *304*, 995–999.

[77] Smith, J. D.; Cappa, C. D.; Wilson, K. R.; Cohen, R. C.; Geissler, P. L.; Saykally, R. J. Unified description of temperature-dependent hydrogen-bond rearrangements in liquid water. *Proceedings of the National Academy of Sciences* **2005**. *102*, 14171–14174.

[78] Prendergast, D.; Galli, G. X-ray absorption spectra of water from first principles calculations. *Phys. Rev. Lett.* **2006**. *96*, 215502.

[79] Pratt, L. R.; Pohorille, A. Theory of hydrophobicity: Transient cavities in molecular liquids. *Proceedings of the National Academy of Sciences* **1992**. *89*, 2995–2999.